*J. Astrophys. Astr.* (2023)44:74
https://doi.org/10.1007/s12036-023-09962-8



# Diving deep into the milky way using anti-reflection coatings for astronomical CCDs

ANMOL AGGARWAL[1,†], ASHI MITTAL[1,†], GEORGE M. SEABROKE[2] and NITIN K. PURI[1,*]

[1]Advanced Sensor Laboratory and Nanomaterials Research Laboratory, Department of Applied Physics, Delhi Technological University, Delhi 110042, India.
[2]Mullard Space Science Laboratory, Department of Space and Climate Physics, Faculty of Maths and Physical Sciences, University College London, London RH5 6NT, UK.
*Corresponding author. E-mail: nitinkumarpuri@dtu.ac.in; nitinpuri2002@yahoo.co.in

MS received 28 December 2022; accepted 8 May 2023

**Abstract.** We report two anti-reflection (AR) coatings that give better quantum efficiency (QE) than the existing AR coating on the Gaia astrometric field (AF) charged coupled devices (CCDs). Light being the core of optical astronomy is extremely important for such missions, therefore, the QE of the devices that are used to capture it should be substantially high. To reduce the losses due to the reflection of light from the surface of the CCDs, AR coatings can be applied. Currently, the main component of the Gaia satellite, the AF CCDs use hafnium dioxide ($HfO_2$) AR coating. In this paper, the ATLAS module of the SILVACO software has been employed for simulating and studying the AF CCD pixel structure and several AR coatings. Our findings suggest that zirconium dioxide ($ZrO_2$) and tantalum pentoxide ($Ta_2O_5$) will prove to be better AR coatings for broadband astronomical CCDs in the future and will open new avenues to understand the evolution of the milky way.

**Keywords.** Gaia—SILVACO TCAD—astronomical instrumentation—charged coupled devices—anti-reflection coatings.

## 1. Introduction

To enrich astronomy with more precise measurements, the European Space Agency (ESA) launched Gaia Satellite in the L2 orbit in December 2013. Its two telescopes keep an eye on millions of stars, galaxies and solar system objects to produce high-precision astrometric and spectroscopic measurements (Prusti *et al*. 2016). The continuous scan gives data sets that are repeatedly reduced to calculate the parallax, position and proper motion of the celestial objects that are observed by the satellite (Crowley *et al*. 2016). The focal plane of the Gaia satellite contains 106 custom-built charged coupled devices (CCDs). These CCDs were designed and manufactured by e2v technologies, UK (Walker *et al*. 2008).

Gaia CCDs were fabricated by e2v in three different variants: astrometric field (AF), red photometer (RP) and blue photometer (BP); each of these are optimized for different wavelength ranges (De Bruijne 2012). The AF CCDs are built using silicon (Si) as a substrate with an anti-reflection (AR) coating, which has a maximum photon absorption for a light of 650 nm; this CCD has an extensive wavelength detection range of 330–1050 nm (Seabroke *et al.* 2008). There are 78 AF CCDs on the Gaia focal plane, which are 16 μm thick (Crowley *et al*. 2016). The BP and RP are enhanced CCDs that have exceptional sensitivity towards the blue (330–680 nm) and red (640–1050 nm) regions of the light spectrum, respectively. Seven BP CCDs present on the Gaia focal plane, have the maximum photon absorption for the light of 360 nm because of its AR coating (Crowley *et al*. 2016). Correspondingly, seven RP CCDs have the maximum photon absorption for the light of 750 nm (Crowley

†First two authors have equal contribution to this research.

Published online: 21 July 2023

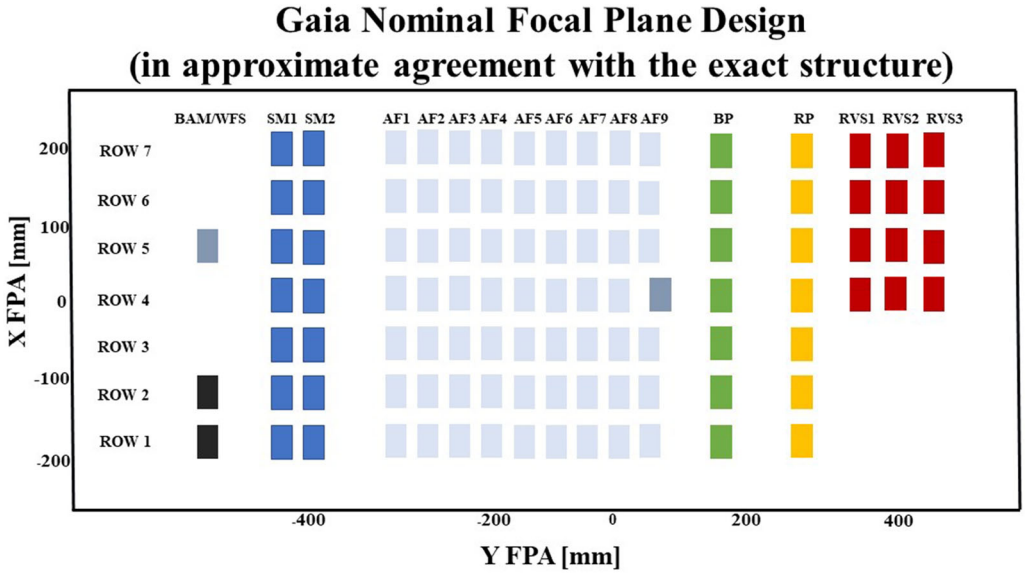


**Figure 1.** Gaia focal plane has 106 CCDs arranged in seven different rows. The red rectangles represent radial velocity spectrometers (RVS). The green and yellow rectangles depict blue and red photometers (BP and RP), respectively, while the grey and black rectangles show wavefront sensors (WFS) and basic angle monitors (BAM), respectively. The light blue rectangles depict the most abundant i.e., AF CCDs and the dark blue rectangles are called sky mappers (SM). The SM and the WFS are also AF CCDs. The RVS and BAM have a construction similar to the RP.

*et al*. 2016). These CCDs have an image area of 4500 lines × 1966 columns (here, lines and columns, refer to the rows and columns of the pixels of the CCD, respectively) (De Bruijne 2012). A schematic diagram of the arrangement of CCDs on the actual Gaia focal plane is shown in Figure 1. The detectors are operating in the time delay and integration mode with a period of 982.8 μs, which synchronizes their line transfer rate with the satellite rotation rate (Crowley *et al*. 2016; De Bruijne 2012). In Gaia parlance, line transfer means electrons being transferred in a row of pixels (Crowley *et al*. 2016).

As the name suggests, AR coatings are essentially important in improving the internal quantum efficiency (IQE) of the CCDs because they play a vital role in enhancing their photon absorption by reducing the losses due to the reflection of incident light. The IQE is used as a measuring stick to determine the performance of an AR coating, which is the ratio of the number of photons that enter the CCD to the number of photons incident on the device (Devi *et al*. 2012). The external quantum efficiency (EQE) is the ratio of the number of photoelectrons generated to the number of photons incident on the CCD (Devi *et al*. 2012). Since the Gaia CCDs generally do not get a lot of time to capture the incoming light from distant objects, their IQE should be substantially high. An AR coating is a thin layer of high refractive index material (Lesser 1987). It also acts as a line of defence for the CCDs (Lesser 1994).

The Gaia AF CCDs have been analysed since they cover the maximum area (78 out of 106 CCDs) of the Gaia focal plane and capture the widest wavelength range. Studies that amalgamate AR coatings and astronomical CCDs have been conducted. IQE of the device has been deliberated, which in fact is directly proportional to the EQE of the device. Several AR coatings for the Gaia AF CCDs have been scrutinized to enhance this factor using the SILVACO software.

## 2. Simulations and calculations

SILVACO TCAD is used to simulate several electronic and optical devices. It uses numerical methods for simulations so that the development and optimization of such devices can be expedited. For simulating the effects of AR coatings on an optoelectronic device, the LUMINOUS and the ATLAS modules of this software can be used.

Since the Gaia AF CCDs are back-illuminated devices, the AR coatings are applied on the backside. Photons are also fired on this side in our simulations. The operating voltage was set to 10 V as suggested by

Seabroke *et al*. (2009). In SILVACO simulations, the ratio of available current density ($J_{available}$) and source current density ($J_{source}$) gives the IQE of a device. The number of photoelectrons generated in a device can be determined using the electron current density ($J_n$).

We simulated an AF CCD pixel in 2-dimensions (2D) using SILVACO, our aim is to obtain IQE of the device with various AR coatings at different wavelengths. We assessed several materials as AR coatings, namely, hafnium dioxide ($HfO_2$), aluminum oxide ($Al_2O_3$), zinc sulfide (ZnS), zirconium dioxide ($ZrO_2$) and tantalum pentoxide ($Ta_2O_5$). Although an AR coating of $HfO_2$ is already present on the AF CCDs (Short *et al*. 2005), which gives impressive results. We suspected that there was a scope of improvement in IQE of the devices. Our simulations proclaim that EQE of the Gaia AF CCDs with this AR coating peaks at 650 nm with a value of 0.99. Simulating these CCDs without any AR coating revealed that there is a large increase of 37.2% in the IQE when AR coatings are applied on such devices. Hence, AR coatings can be regarded as a cornerstone of astronomical CCDs.

A CCD is essentially a MOS-based device, which acts as an image detector. In MOS, the letter M stands for metal, the letter O stands for oxide and the letter S stands for semiconductor (Lundström 1981). Therefore, the structure of CCD consists of a layer of metallic electrodes placed on a thin insulating layer lined over a semiconductor substrate. Lundström (1981) reports details of the MOS structure. CCDs are of two types, front-illuminated and back-illuminated. In the former, light is incident on the electrodes, while the light is incident on the semiconductor substrate in the latter (Lesser 2014, 2015). The back-illuminated CCDs are constructed in actual practice because they offer a larger surface area for photogeneration and photon absorption than front-illuminated CCDs (Lesser 2015).

For simulating the Gaia AF CCD pixel in SILVACO, several structural parameters are required, which are derived from (Seabroke *et al*. 2008, 2009, 2010a, b). The pixel structure of the CCD has three different faces, which is evident from Figure 2. We simulated the structure in the across scan (AC) direction in 2D with a pixel size of 16 μm × 30 μm. The 16 μm thickness of the pixel is subdivided into multiple layers, the details of which are summarized in Table 1.

The Gaia AF CCD entails a lot of interesting structural intricacies, namely, buried channel (BC), supplementary buried channel (SBC) and anti-blooming drain (ABD) (Seabroke *et al*. 2008). A BC is formed near a p–n junction by placing a thin layer of negatively doped Si on a positively doped substrate. This channel has no free charges and is used to hold the photogenerated electrons before they are read out. A photon incident on a CCD creates an electron–hole pair; the electron thus generated, then moves to the BC.

The SBC is a support feature to the BC but is no less functional. When the number of photogenerated electrons exceeds the capacity of the SBC, they spill into the BC, which holds them until they are read out (Seabroke *et al*. 2010a, 2013). The length of BC and SBC runs from 4.5 to 29 μm in the AC direction (Seabroke *et al*. 2010b). The ABD, which is present on either side of the pixel in the AC direction is a

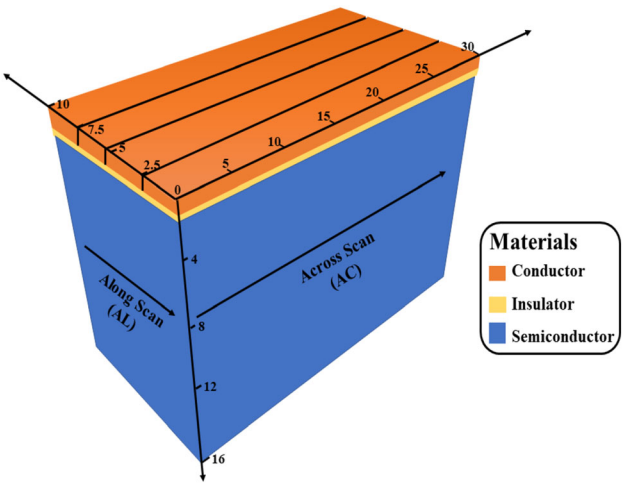


**Figure 2.** Structure of a single pixel of the Gaia AF CCD (all the measurements are in μm).

**Table 1.** Thickness and doping densities of different layers in the AF CCD pixel structure (Seabroke *et al*. 2009).

| Material | Type | Thickness (μm) | Doping density ($cm^{-3}$) |
|---|---|---|---|
| Polycrystalline Si | Conductor | 0–0.5 | 0 |
| Silicon dioxide ($SiO_2$) | Insulator | 0.5–0.63 | 0 |
| N-type Si | Semiconductor | 0.63–1.17 | $2.65 \times 10^{16}$ |
| P-type Si | Semiconductor | 1.17–16 | $1.3 \times 10^{14}$ |

**Table 2.** List of theoretical and experimental constants.

| Name of Constant | Theoretical values used in SILVACO ATLAS | Experimental values |
|---|---|---|
| Energy gap of Si ($E_g$) | 1.08 eV at 300 K<br>1.11 eV at 163 K | 1.12 eV at 300 K (Strehlow & Cook 1973) |
| Relative permittivity of Si ($\varepsilon_r$) | 11.8 at 300 K<br>11.8 at 163 K | 11.66 at 300 K (Krupka *et al.* 2006) |
| Electron affinity of Si ($X$) | 4.17 eV at 300 K<br>4.16 eV at 163 K | 4.05 eV at 300 K (Melnikov & Chelikowsky 2004; Chanana 2022) |
| Temperature ($T$) | 163 K | 163 K (Seabroke *et al.* 2008) |

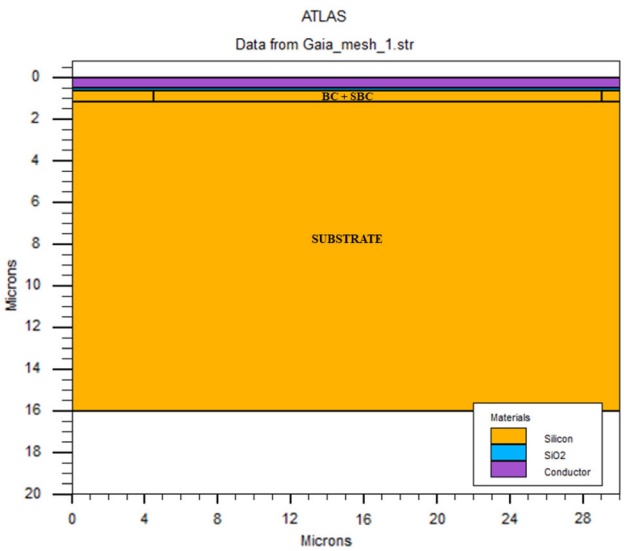


**Figure 3.** 2D Gaia AF CCD structure in the across scan (AC) direction as simulated in SILVACO ATLAS.

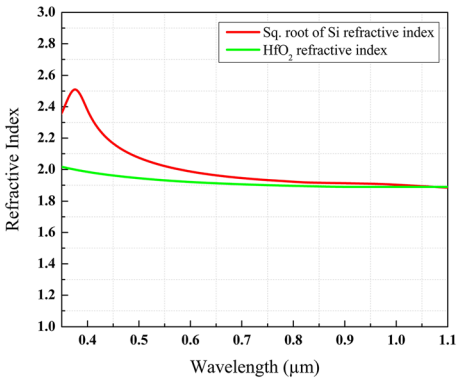


**Figure 4.** Comparison of the refractive index of $HfO_2$ with the square root of the refractive index of Si at different wavelengths.

shielding feature. It prevents the electrons from divulging into the adjacent pixel (Seabroke *et al.* 2010a). Now, to simulate all these interesting features in SILVACO, the whole AF CCD image pixel was modeled with uniform doping as suggested by Seabroke *et al.* (2009).

The Gaia AF CCDs work at a temperature of 163 K (Seabroke *et al.* 2008) to minimize the dark current, which is attributed to the false positive signals produced in the CCD due to the thermal energy of electrons (Lesser 2015). Therefore, to match our theoretical simulations with the experimental results reported by Walker *et al.* (2008), we conducted our simulations at the same temperature.

To simulate the CCD pixel structure, the SILVACO ATLAS package uses some constants for the simulated materials that are handled internally. It uses the Monte Carlo method to model the structure. Table 2 compares the experimental values of the constants with the values used during our simulations.

Figure 3 exhibits the simulated structure of the Gaia AF CCD pixel; the illustration was generated using the TonyPlot tool of the SILVACO software.

## 2.1 *AR coatings*

We have elucidated the Gaia AF CCD pixel structure used in our simulations, but to test their efficiency, the IQE can be used. To begin with, we have focused on single-layer AR coatings that have been applied on the backside of the CCD (substrate side). The thickness of the AR coating is estimated using the quarter wavelength formula (Equation 1):

$$\text{AR coating thickness} = \frac{\lambda}{4n}. \quad (1)$$

In Equation (1), λ is the wavelength at which the AR coating is centered, i.e., the wavelength at which the AR coating will allow for maximum photon absorption; $n$ is the refractive index of the AR coating material at the wavelength λ (Lesser 1987). The SOPRA database of the SILVACO ATLAS software was tremendously helpful in allowing us to include the refractive indices of the AR coatings. When the

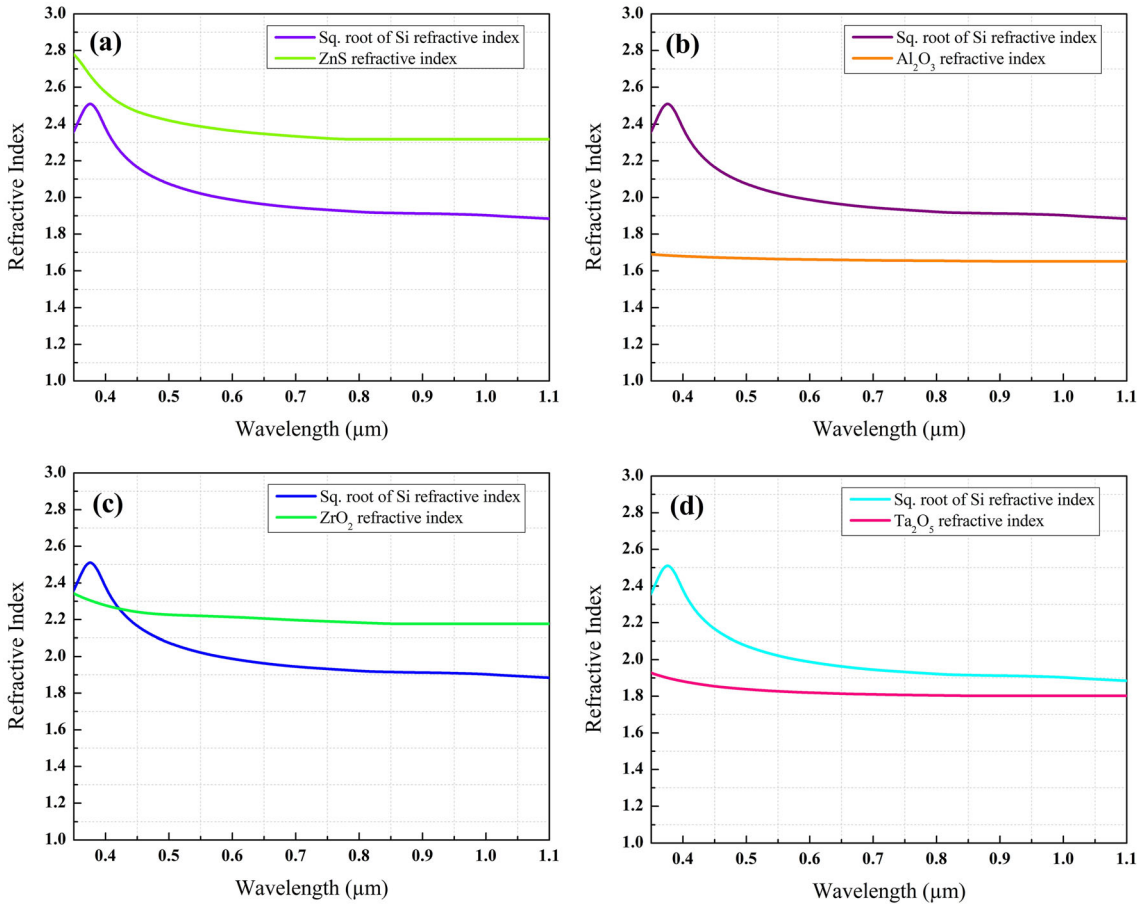


**Figure 5.** Comparison of the square root of the refractive index of Si with (a) ZnS, (b) $Al_2O_3$, (c) $ZrO_2$ and (d) $Ta_2O_5$ at different wavelengths.

refractive index of AR coatings at a specified wavelength comes in approximate agreement with $\sqrt{n}$, where $n$ is the refractive index of the substrate material at that wavelength, then, we get excellent IQE values. To choose an AR coating, this factor was deliberated.

On comparing the values of refractive indices of various AR coatings with the $\sqrt{n}$, at different wavelengths, we got some AR coatings whose refractive indices match the $\sqrt{n}$ values and promise good results in IQE. In Figure 4, we can see the comparison of $HfO_2$ coating's refractive indices with the square root values of Si refractive indices. There is a very good matching which evidently explains why this AR coating is used in designing the Gaia AF CCDs.

On performing the same comparison with various AR coatings, we got some promising results from ZnS, $Al_2O_3$, $ZrO_2$ and $Ta_2O_5$, which can be seen in Figure 5. Figure 5(a) shows how similar are the values of $\sqrt{n}$ of Si and the refractive index of ZnS. Figure 5(b) shows that the refractive index of $Al_2O_3$ is also close to the $\sqrt{n}$ of Si values. Figure 5(c) and (d) show similar results for $ZrO_2$ and $Ta_2O_5$.

While choosing the materials for AR coatings, their imaginary refractive index, which is a complex optical constant, often referred to as the extinction coefficient has also been considered. Using this, we can calculate the absorption coefficient ($\alpha$), which is the distance a photon can travel into the material before being absorbed. It is given by Equation (2):

$$\text{Absorption coefficient } (\alpha) = \frac{4\pi k}{\lambda}, \tag{2}$$

where $\lambda$ is the wavelength of incident light. We calculated the values of $\alpha$ for whole wavelength range of the Gaia astrometric field (AF) CCD using SILVACO ATLAS with different AR coatings, which are presented in Figure 6(a–c). It can be concluded from these results that the AR coatings have no effect on the absorption coefficient of silicon (Si).

Another factor that has been deliberated while selecting the AR coating material is reflectivity ($R_0$).

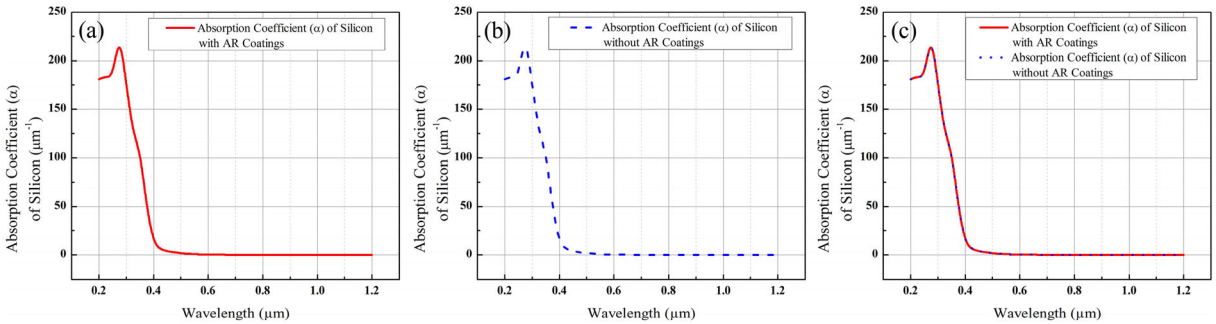


**Figure 6.** Absorption coefficient of Si: (a) with AR coatings, (b) without AR coatings and (c) with and without AR coatings.

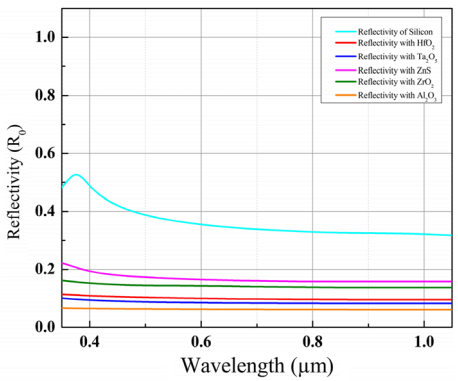


**Figure 7.** Reflectivity of the CCD surface without any AR coating and with different AR coatings.

Equation (3) is used to calculate the reflectivity of a surface using the real refractive indices:

$$\text{Reflectivity } (R_0) = \left|\frac{n_1 - n_2}{n_1 + n_2}\right|^2, \tag{3}$$

where $n_1$ and $n_2$ are the real refractive indices (at a specific wavelength) of the medium from which the light is incident and the AR coating material, respectively. The reflectivity of the Si–air interface is largely affected by the optical properties of AR coating materials. The effect of AR coatings on the reflectivity of the Si–air interface is presented in Figure 7, which has been calculated using the SILVACO ATLAS software.

For an AR coating to perform well, its respective refractive indices of the AR coating material also should be in approximate agreement with the square root of the respective refractive indices of the substrate material ($\sqrt{n}$), as per Lesser (1987). $Ta_2O_5$ satisfies this condition and it is the best among all the studied AR coating materials, and reduces the reflectivity substantially. Hence, it can be concluded that $Ta_2O_5$ can be proven to be the best AR coating material for our case. Although $Al_2O_3$ reduces the reflectivity to the least value compared to all the studied AR coatings, as presented in Figure 7, its respective refractive indices are not very close to the square root of the respective refractive indices of Si (Figure 5b), which might hinder its performance.

## 3. Results and discussion

While simulating the pixel structure with the $HfO_2$ AR coating, Equation (1) deduces the thickness of the coating to 0.085 μm. We identified the EQE for this setup to benchmark our simulations against the previously published EQE values by Walker *et al*. (2008). The simulation results are comparable to the experimental results, which can be visualized in Figure 8(a). Any differences in the values of EQE might be because of the absence of ABD in our structure, as the parameters required for its simulations were not published in the current literature.

On calculating IQE for the Gaia AF CCD without applying any AR coating, it was discovered that they have a maximum IQE of 0.65 at the wavelength of 0.7 μm. Comparing the IQE of the CCDs with and without the $HfO_2$ coating, we clearly observed an average increment of about 37.2% in the whole wavelength range. Figure 8(b) coveys this increment graphically.

As per our study of AR coating materials, we choose four AR coatings to test our device. One of them is ZnS. Application of 0.069 μm thick single-layer coating of ZnS, centered at 0.65 μm, unfolds that it is not very suitable for our device. The IQE curve in Figure 8(c) outlines that there is an average decrement of $\sim$3.5% when studied parallel to the Gaia AF CCD with a $HfO_2$ AR coating in the whole range.

Our next choice was $Al_2O_3$. Therefore, we applied a single layer of it with a thickness of about 0.098 μm (calculated as per Equation 1), centered at 0.65 μm. The Gaia AF CCD with $HfO_2$ AR coating still

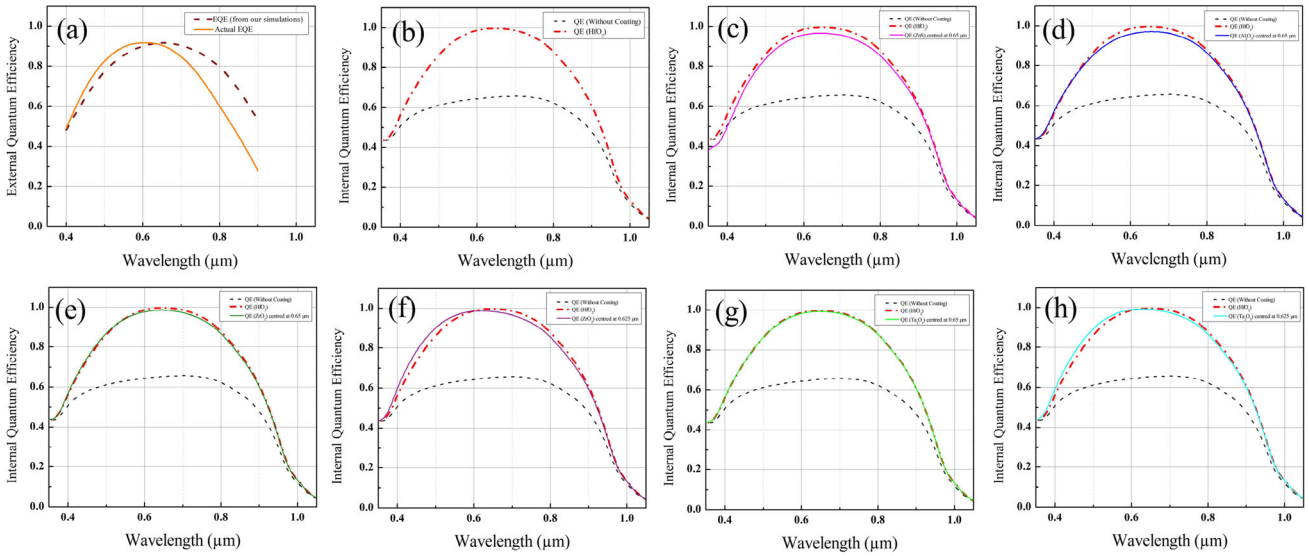


**Figure 8.** (a) EQE of the Gaia AF CCDs derived from our simulations and the actual EQE reported by Walker *et al.* (2008). The IQE versus wavelength graph for Gaia AF CCD, (b) without an AR coating and with a $HfO_2$ coating (centered at 0.65 μm), (c) ZnS coating (centered at 0.65 μm), (d) $Al_2O_3$ coating (centered at 0.65 μm), (e) $ZrO_2$ coating (centered at 0.65 μm), (f) $ZrO_2$ coating (centered at 0.625 μm), (g) $Ta_2O_5$ coating (centered at 0.65 μm) and (h) $Ta_2O_5$ coating (centered at 0.625 μm).

**Table 3.** Percentage increment and decrement in QE of the Gaia AF CCD with different AR coatings as compared to the $HfO_2$ AR coating.

| AR coatings | Wavelength range (μm) | Percentage increment/decrement in IQE | Average increment/decrement in IQE |
|---|---|---|---|
| $HfO_2$ | 0.33–1.05 | Increment (2.6–53.3%) as compared to a CCD without any AR coating | Increment (37.2%) as compared to a CCD without any AR coating |
| ZnS (centered at 0.65 μm) | 0.35–1.05 | Decrement (0.3–12.2%) as compared to $HfO_2$ | Decrement (3.5%) as compared to $HfO_2$ |
| $Al_2O_3$ (centered at 0.65 μm) | 0.35–0.425 | Increment (0.1–2.3%) as compared to $HfO_2$ | Increment (1.3%) as compared to $HfO_2$ |
| | 0.425–1.05 | Decrement (0.09–2.8%) as compared to $HfO_2$ | Decrement (1.9%) as compared to $HfO_2$ |
| $ZrO_2$ (centered at 0.65 μm) | 0.4–0.525 | Increment (0.04–1.35%) as compared to $HfO_2$ | Increment (0.8%) as compared to $HfO_2$ |
| | 0.525–1.05 | Decrement (0.19–1.4%) as compared to $HfO_2$ | Decrement (1.1%) as compared to $HfO_2$ |
| $ZrO_2$ (centered at 0.625 μm) | 0.375–0.575 | Increment (0.63–6.85%) as compared to $HfO_2$ | Increment (4%) as compared to $HfO_2$ |
| | 0.575–1.05 | Decrement (0.38–2.72%) as compared to $HfO_2$ | Decrement (2%) as compared to $HfO_2$ |
| $Ta_2O_5$ (centered at 0.65 μm) | 0.35–0.9 | Decrement (0.64% and less) as compared to $HfO_2$ | No prominent change as compared to $HfO_2$ |
| | 0.9–1.05 | Increment (0.04% and less) as compared to $HfO_2$ | No prominent change as compared to $HfO_2$ |
| $Ta_2O_5$ (centered at 0.625 μm) | 0.375–0.6 | Increment (0.17–5.15%) as compared to $HfO_2$ | Increment (2.8%) as compared to $HfO_2$ |
| | 0.6–1.05 | Decrement (0.19–1.57%) as compared to $HfO_2$ | Decrement (1.2%) as compared to $HfO_2$ |

provides better results for most wavelengths as compared to $Al_2O_3$. It is also observed that $Al_2O_3$ coating provides an average improvement in IQE of about 1.3% in the 0.35–0.425 μm range and an average decrement of about 1.9% in the rest of the wavelength range. These results are compiled in the graph presented in Figure 8(d).

The next alternative that we analysed was a single-layer coating of $ZrO_2$ centered at 0.65 μm. The thickness of the coating was set as per Equation (1) close to 0.073 μm. After observing the graphical data presented in Figure 8(e), we infer that there is an average increment in the IQE of around 0.8% in the range of 0.4–0.525 μm when analogized with the IQE values when $HfO_2$ coating was applied. For the rest of the wavelengths, the AR coating of $HfO_2$ offers an average increment of almost 1.1%, when compared to $ZrO_2$.

Inspired by the improvements shown by $ZrO_2$, we adjusted its thickness to an approximate value of 0.071 μm, which allows for a peak absorbance of the light of wavelength of 0.625 μm. Our experimentation on this, yields an average increment of nearly 4% for the wavelength range of 0.375–0.575 μm when compared with $HfO_2$, with an average compromise of around 2% in the wavelength range of 0.575–1.05 μm. This data is visualized in Figure 8(f).

We concluded our studies with $Ta_2O_5$, which is a promising AR coating. A single layer of $Ta_2O_5$, centered at 0.65 μm with a thickness of $\sim$0.09 μm (calculated using Equation 1), permits almost the same performance as $HfO_2$. It is evident from Figure 8(g) that the two curves virtually overlap each other in the whole range. We did not obtain such promising results for any other AR coating. Hence, to improve the IQE in the low wavelength region, we deposited a 0.086 μm thick layer of $Ta_2O_5$ to the center of the AR coating at 0.625 μm. The IQE of the Gaia AF CCDs with an AR coating of $Ta_2O_5$ shows an average increment of about 2.8% compared to the CCDs with $HfO_2$ AR coating in the wavelength range of 0.375–0.6 μm. There is an average decrease of around 1.2% in IQE of the wavelengths ranging from 0.6 μm to 1.05 μm, which is clearly evident in Figure 8(h).

A comparative study has been drawn to analyse, which AR coating best suits the Gaia AF CCDs. It is observed that a single layer coating of $ZrO_2$ and $Ta_2O_5$ gives similar or better results as compared to $HfO_2$ for most wavelengths lying in Gaia's AF CCD range (330–1050 nm) (Seabroke *et al*. 2008). Table 3 summarizes the comparison among the IQE of CCDs for different AR coatings.

## 4. Conclusions

We tested our Gaia AF CCD pixel model against the actual EQE values reported by Walker *et al.* (2008), which indicated the accuracy of our simulations. We presented our studies of the Gaia AF CCDs with various AR coatings to enhance the QE values. Any deviations in the results might be attributed to the absence of SBC and ABD in our structure since these features are proprietary to e2v. The performance of an AR coating can also be determined using a simple Si wafer. But, to validate our results for astronomical CCDs, we used an electrical model in SILVACO ATLAS. This allows our results to be more acceptable to the astronomical community.

Our simulations establish that AR coatings are an important factor in improving the IQE and EQE of astronomical CCDs. They also elucidate that $Ta_2O_5$ and $ZrO_2$ are better materials for astronomical CCDs than $HfO_2$, mainly in the spectrum region from 0.330 μm to 0.575 μm. Hence, this work has important implications for the development of astronomical CCDs, which will help them to obtain the best possible data from satellites and telescopes. Multi-layer AR coatings can be deliberated for this purpose in the future, which might enhance our knowledge of the Milky Way even more.

## Acknowledgments

We are grateful to Prof. Ashutosh Bharadwaj, University of Delhi, for his help and motivation throughout this research. We are also thankful to Dr Harsupreet Kaur for providing us with the license for TCAD SILVACO ATLAS 2021 software. We gratefully acknowledge Dr Ritika Khatri, Delhi Technological University, for her continuous support and guidance during this research.

## References

Chanana R. K. 2022, Journal of Electrical and Electronics Engineering 17, 09
Crowley C., Kohley R., Hambly N. C. *et al*. 2016, A&A 595, A6
De Bruijne J. 2012, Ap&SS 341, 31
Devi H. R., Bisen O. Y., Nanda S., Nandan R., Nanda K. K. 2021, Current Science 00113891, 127
Krupka J., Breeze J., Centeno A. *et al*. 2006, IEEE Transactions on Microwave Theory and Techniques 54, 3995
Lesser M. 1987, Optical Engineering 26, 911
Lesser M. 2014, in High Performance Silicon Imaging (Elsevier), p. 78
Lesser M. 2015, PASP 127, 1097
Lesser M. P. 1994, in Instrumentation in Astronomy VIII, Vol. 2198, SPIE, p. 782
Lundström I. 1981, Sensors and Actuators 1, 403
Melnikov D. V., Chelikowsky J. R. 2004, Physical Review B 69, 113305
Prusti T., De Bruijne J., Brown A. G. *et al*. 2016, A&A 595, A1
Seabroke G., Holland A., Burt D., Robbins M. 2009, in Astronomical and Space Optical Systems, Vol. 7439, SPIE, p. 35
Seabroke G., Holland A., Burt D., Robbins M. 2010a, in High Energy, Optical, and Infrared Detectors for Astronomy IV, Vol. 7742, SPIE, p. 339

Seabroke G., Holland A., Cropper M. 2008, in High Energy, Optical, and Infrared Detectors for Astronomy III, Vol. 7021, SPIE, p. 515

Seabroke G., Prod'homme T., Hopkinson G. *et al.* 2010b, European Astronomical Society Publications Series 45, 433

Seabroke G., Prod'homme T., Murray N. *et al.* 2013, MNRAS 430, 3155

Short A., Hopkinson G., Laborie A. *et al.* 2005, in Focal Plane Arrays for Space Telescopes II, Vol. 5902, SPIE, p. 31

Strehlow W., Cook E. L. 1973, Journal of Physical and Chemical Reference Data 2, 163

Walker A., Eaton T., Steward R. *et al.* 2008, in Sensors, Systems, and Next Generation Satellites XII, Vol. 7106, SPIE, p. 390